NMR IN BIOMEDICINE
NMR Biomed. 2004;**17**:181–190
Published online in Wiley InterScience (www.interscience.wiley.com). DOI:10.1002/nbm.887

In vivo elasticity measurements of extremity skeletal muscle with MR elastography

Kai Uffmann,* Stefan Maderwald, Waleed Ajaj, Craig G. Galban, Serban Mateiescu, Harald H. Quick and Mark E. Ladd

Department of Diagnostic and Interventional Radiology, University Hospital Essen, Germany

Received 17 September 2003; Revised 14 April 2004; Accepted 20 April 2004

ABSTRACT: MR elastography (MRE) has been shown to be capable of non-invasively measuring tissue elasticity even in deep-lying regions. Although limited studies have already been published examining *in vivo* muscle elasticity, it is still not clear over what range the *in vivo* elasticity values vary. The present study intends to produce further information by examining four different skeletal muscles in a group of 12 healthy volunteers in the age range of 27–38 years. The examinations were performed in the biceps brachii, the flexor digitorum profundus, the soleus and the gastrocnemius. The average shear modulus was determined to be 17.9 (±5.5), 8.7 (±2.8), 12.5 (±7.3) and 9.9 (±6.8) kPa for each muscle, respectively. To ascertain the reproducibility of the examination, the stiffness measurements in two volunteers were repeated seven times for the biceps brachii. These examinations yielded a mean shear modulus of 11.3 ± 1.7 and 13.3 ± 4.7 kPa for the two subjects. For elasticity reconstruction, an automated reconstruction algorithm is introduced which eliminates variation due to subjective manual image analysis. This study yields new information regarding the expected variation in muscle elasticity in a healthy population, and also reveals the expected variability of the MRE technique in skeletal muscle.

KEYWORDS: elasticity; elastography; skeletal muscle; MRI

INTRODUCTION

Many pathologies and injuries can potentially cause a change in muscle tissue elasticity (stiffness). Therefore, the *in vivo* measurement of elastic properties could be a valuable addition to muscle diagnosis and therapy monitoring. Unfortunately, techniques to non-invasively quantify tissue elasticity are limited. Ultrasound sonoelasticity has been used to measure muscle elasticity,[1] but has limitations on the range of resolvable elasticity values.

Magnetic resonance elastography (MRE) is a relatively new technique which uses a phase contrast acquisition to monitor tissue motion in response to external vibration.[2,3] As demonstrated by several studies, MRE provides the potential for quantitative determination of tissue elasticity in various regions of the body,[4,5] including deeper-lying regions not accessible for external palpation. It has been demonstrated, for example, that breast tumors may be detected and visualized by their higher elasticity values relative to the surrounding healthy tissue.[6,7] Additionally it has been shown that elasticity changes in the biceps brachii[8,9] or in the calf muscles[10] under isometric load are measurable by MRE.

It is known that several diseases either directly, such as dystrophy, or indirectly, such as stroke, polyneuropathy, arthritis, peripheral vascular disease (PVD) and chronic obstructive pulmonary disease (COPD), influence the structure of muscle tissue. Disuse of muscle due to operative interventions or injury can also lead to atrophy. Therefore, it might be useful to have a tool to non-invasively and quantitatively monitor muscle elasticity.

Various diagnostic methods are available to investigate specific influences on muscles. The most obvious diagnosis of muscle is based on the subjective rating of muscle tone or 'fitness' by a physician, a physiotherapist or even the patient. Intuitively, the tonus is related to muscle stiffness, but is non-quantitative. Other diagnostic means which are available for examining muscle include electromyography, biopsy, MR spectroscopy (MRS), biochemical examinations of blood and urine, conventional MR imaging (MRI) and ultrasound. Although each of these methods can reveal particular aspects of muscle disease and injury, none is capable of providing a complete picture.

MRS yields a microscopic view of muscle cell structure and the cell environment by quantifying the concentration of certain molecules or ions. MRI gives macroscopic insight into the muscle tissue. Detection of

**Correspondence to:* K. Uffmann, Department of Diagnostic and Interventional Radiology, University Hospital Essen, OZ II, Hufelandstr. 55, D-45122 Essen, Germany.
E-mail: kai.uffmann@uni-essen.de

Abbreviations used: COPD, chronic obstructive pulmonary disease; DSP, digital signal processing; MR, magnetic resonance; MRE, magnetic resonance elastography; MRI, magnetic resonance imaging; PVD, peripheral vascular disease; MRS magnetic resonance spectroscopy; *TR*, repetition time.

tissue damage or alteration in morphologic images is often sufficient to clarify the cause of muscle dysfunction. In addition, MRI can offer measurements of volume, perfusion, diffusion,[11] and changes in magnetization relaxation (e.g. T_1 or multicomponent T_2 relaxation)[12,13] due to physiological and biochemical processes.

The possible combination of these MRS and MRI examinations with MRE could allow a completely non-invasive, comprehensive evaluation of muscle status with a single examination modality. As a starting point, elasticity values in normal tissue for various muscle groups need to be established, so that the effect of various disease processes and injuries on muscle elasticity can be investigated relative to baseline healthy tissue. Thus far, *in vivo* values in the literature are only available for a limited number of muscles and for a limited number of subjects.[1,8,9,10,14] The goal of this study was therefore to collect quantitative elasticity values in four different peripheral skeletal muscles under unloaded conditions in healthy volunteers. These data are used to evaluate the variability of MRE measurements in skeletal muscle.

As there is no general agreement on the most suitable reconstruction algorithm for calculating elasticity values in muscle, an automated method based on published reconstruction methods[6] is introduced and discussed. This algorithm should overcome problems arising with the subjective manual analysis of phase images used in previous MRE studies.[8–10] The manual measurement of wavelengths in the acquired phase images is particularly difficult within the small sections of muscle available, where complex wave patterns occur.

Finally, the study results should be used to advance the evaluation of MRE as a diagnostic method for muscle disease and injury.

METHODS

MRE system

The MRE examinations were performed on a 1.5 T scanner (Sonata, Siemens, Erlangen, Germany). The mechanical excitation of the muscle tissue was realized by a custom-designed piezoelectric actuator.[15] The imaging sequence was a modified phase contrast gradient echo sequence equipped with sinusoidal motion sensitizing gradients. The mechanical oscillation was generated in phase with the motion-sensitizing gradients. Stability of the phase relationship was maintained by a trigger which was sent every repetition time (*TR*) from the MR scanner to a digital signal processing (DSP) card in a PC. The DSP card synchronized the control voltage for driving the piezoelectric ceramic in the actuator to the trigger signal.

For a complete dataset, three adjacent slices were acquired with eight equidistant phase offsets between the mechanical vibration and the motion-sensitizing gradients.

Elasticity reconstruction/agar phantom

An automated reconstruction algorithm was implemented to overcome subjective variations owing to manual measurement of wavelengths in the phase images. The algorithm used for *in vivo* muscle elasticity calculation is introduced by the reconstruction of a phantom consisting of two compartments with agar gel of 1 and 2% concentration [Fig. 1(A)]. The excitation frequency for the phantom experiment was 250 Hz. For comparison, the wave vector was also measured manually in the spatial phase reconstructed with a sinusoidal fit over different phase offsets. Additionally, a manual measurement of the wavelength in each of the eight phase offsets was performed, similar to the technique used, for example, in Dresner *et al.*[8] and Uffmann *et al.*[9]

Assuming that the spin displacement u is oriented only along the spatial direction parallel to the actuator motion, it can then be described in complex notation by $u = A \cdot e^{i(\omega t+\varphi_0)} \cdot e^{i\varphi}$, where A is the amplitude, $\omega = 2\pi f$ with f the oscillation frequency, φ the spatial phase, and φ_0 a phase offset.

The phase images acquired at 8 different phase offsets $\varphi_0 \in (0°, 45°, 90°, 135°, 180°, 225°, 270°, 315°)$ can be interpreted as images at eight different time points. The eight different phase offsets subdivide one cycle of the spin oscillation into equal parts, where one cycle is of duration $T = 1/f$ and the acquisition corresponds to sampling the oscillation cycle at eight different time points. Figure 1(B) shows strips through all eight phase images from the same region. The data in all pixels plotted over the eight phase offsets yield a sinusoidal phase change due to $\omega t + \varphi_0$. Thus, the spatial phase φ can be reconstructed by fitting a sinusoid to the eight data points. The frequency of the sinusoid was assumed to match the frequency of mechanical vibration f.

The spatial phase, as given by $\varphi = \vec{k} \cdot \vec{r}$, with $\vec{k}$ the wave vector and $\vec{r}$ the position vector, varies from one pixel to the next depending on the spatial propagation of the waves, which is determined by the medium elasticity. Figure 1(C) shows the spatial phase $\varphi = \vec{k} \cdot \vec{r}$ along a vertical line centered through the phantom. The components of the wave vector were calculated by the spatial derivative of the phase along each spatial direction. The highest contribution resulted from in-plane changes along the image rows and columns, while the spatial phase remained almost constant from slice to slice. In this way, the resulting wave vector points in the direction of the maximum slope of the spatial phase. The magnitude of the wave vector yielded a wavelength λ for each pixel as given by $\lambda = 2\pi/|\vec{k}|$. The elasticity, represented by the shear modulus, μ, could then be calculated from $\mu = \rho \cdot (\lambda \cdot f)^2$, where ρ is the tissue density and f the excitation frequency.[16] This formula is valid for extended, Hookean, isotropic media.

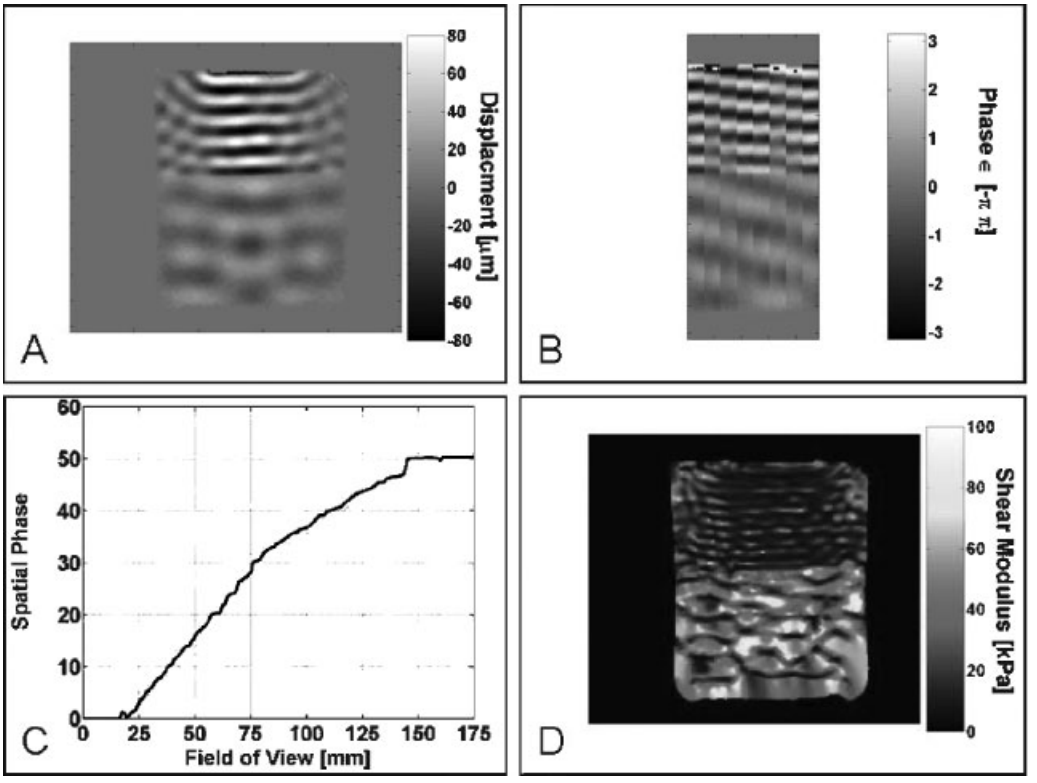

Figure 1. (A) Phase image acquired in a phantom with 1% agar gel in the upper half and 2% agar gel in the lower half. The phase is scaled to displacement. The FOV is $200 \times 175\,\mathrm{mm}^2$. (B) Central vertical strips through each of the eight phase images acquired with phase offsets of 0, 45, 90, 135, 180, 225, 270, and 315°. For each pixel, the values across phase offsets show a sinusoidal characteristic. (C) Profile of the spatial phase obtained by the sinusoidal fit over all eight phase offsets. The border between compartments with different agar gel concentration is located at 80 mm from the field of view. (D) Elastogram of the two-compartment phantom. The upper half and the lower half yield a mean shear modulus of 12.4 and 37.9 kPa, respectively. The white lines show the ROIs used for determination of the mean values in each compartment

Test image

The reconstruction algorithm was additionally checked with a test image [Fig. 2(A)]. The test image contains wave patterns propagating in one spatial direction with a wave number k of $310\,\mathrm{m}^{-1}$ surrounding a rectangular region with a wavenumber k of $207\,\mathrm{m}^{-1}$. At an excitation frequency of $f = 1/0.007\,\mathrm{s} = 142.9\,\mathrm{Hz}$ and assuming

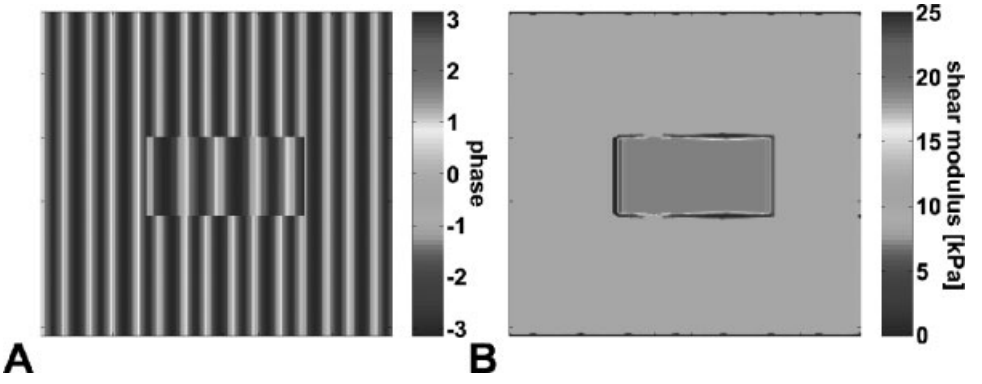

Figure 2. (A) Test data simulating a phase image containing different wave patterns and (B) the reconstructed elastogram. The test object consists of two regions containing horizontal wave patterns with a wavelength of 30.4 mm in the centered square and 20.3 mm in the surrounding area, corresponding to shear moduli of 18.8 and 8.4 kPa, respectively

tissue density of $\rho = 1000\,\mathrm{kg/m^3}$, this corresponds to a region with a shear modulus of $\mu = 18.8\,\mathrm{kPa}$ surrounded by softer tissue with a shear modulus of $\mu = 8.4\,\mathrm{kPa}$.

Assuming these shear moduli for the inclusion and the background, the phase data for the test image were calculated from:[2]

$$\phi(r,\theta) = \frac{1}{2}\gamma NT(\vec{G}\cdot\vec{\xi}_0)\cos(\vec{k}\cdot\vec{r}+\theta)$$

where ϕ is the phase, θ the phase offset between excitation oscillation and the sinusoidal (motion-sensitizing) gradients, γ the gyromagnetic ratio for H^+, N the number of sinusoidal gradient cycles, T the gradient period, $\vec{G}$ the vector of the sinusoidal gradients, $\vec{\xi}$ the spin displacement vector, $\vec{k}$ the wave vector, and $\vec{r}$ the position vector.

In vivo examinations

For the skeletal muscle elasticity measurements, the biceps brachii, the flexor digitorum profundus, the soleus and the gastrocnemius lateralis of 12 healthy young volunteers were examined with MRE. For the examination of the flexor digitorum profundus, only 11 volunteers were available.

The group consisted of eight male and four female healthy individuals in the age range 27–38 years (31 ± 5 years). To check reproducibility and measurement variance, the biceps brachii of two volunteers (32 and 27 years old) were examined seven times with the same setup on six separate days over an 8 month period.

The vibrating lever of the mechanical actuator was placed on a tendon of the muscle. Excitation frequencies of 142 and 100 Hz were used for the upper and lower extremity muscles, respectively. These frequencies were determined in preliminary experiments as being most suitable for excitation of the different muscle groups to obtain the highest possible amplitude in the phase images. The vibration amplitude of the lever was in the range 600–700 μm. The sequence parameters were: $TR = 84\,\mathrm{ms}$, $TE = 24.6\,\mathrm{ms}$, matrix = 256×192, FOV = $20 \times 15\,\mathrm{cm^2}$ for 142 Hz excitation, and $TR = 120\,\mathrm{ms}$, $TE = 33.3\,\mathrm{ms}$, matrix = 256×144, FOV = $28 \times 21\,\mathrm{cm^2}$ for 100 Hz excitation. The flip angle was 15° and the read-out bandwidth was 256 Hz/pixel at both frequencies. The slice thickness was 5 mm.

Patient positioning and the acquisition of anatomical images as well as the complete elastography dataset with 24 images lasted approximately 20 min. The elastography images were oriented coronally through the muscles. With the aid of a custom-made positioner, the actuator could be flexibly positioned for the excitation of each muscle. Figure 3 shows the setup for imaging of the calf muscle. The elasticity of the gastrocnemius and the soleus was determined from a common dataset. The slices for acquisition in the calf were oriented to intersect both muscles.

Figure 3. Setup using a transmit–receive extremity coil for examination of the calf muscles, i.e. the gastrocnemius and the soleus. Apart from RF coil used and positioning of the actuator, the same principle setup was used for examination of the biceps and the forearm

For the reconstruction of the *in vivo* data, a tissue density of $\rho = 1100\,\mathrm{kg/m^3}$ [17] was assumed. A region of interest (ROI) for elasticity calculation was manually chosen from the magnitude images showing the muscle anatomy. The elasticity values in this ROI were then averaged under the assumption that the muscle tissue is homogeneous. The wave patterns in the phase images were additionally taken into consideration to exclude areas at muscle boundaries where the complexity of the wave patterns is extreme due to reflections and refraction. Also, regions with phase wraps were excluded. Where possible, the ROI was chosen to include several wave cycles in the phase images.

A Fisher-PLSD test was used to calculate p-values for all possible combinations of the data groups biceps, flexor digitorum profundus, gastocnemius, soleus, upper extremity and lower extremity, for both the entire population and for the male and female subpopulations. A p-value smaller than 0.05 was considered to be statistically significant.

Finally, correlations were sought between muscle stiffness and the height or weight of the subject by producing scatter plots and determining Pearson correlation coefficients for both the overall group and individually for the

male and female subgroups. For the correlation analysis, the shear modulus values for each muscle separately were plotted vs height and weight, both independent of and dependent on gender.

RESULTS

Agar phantom

Reconstruction yielded a mean shear modulus of 12.4 ± 5.1 kPa for the upper 1% agar gel compartment and 37.9 ± 6.4 kPa for the lower 2% agar gel compartment of the phantom [Fig. 1(D)]. Manual slope determination of the reconstructed spatial phase as shown in Fig. 1(C) yielded wave vectors of 475.6 and 242.1 m^{-1} for the upper and lower compartments, respectively. With an assumed density of 1000 kg/m^3 and an excitation frequency of 250 Hz, this results in shear moduli of 10.9 and 42.1 kPa, respectively. Finally, manual measurement of the wavelength in each of the eight phase images resulted in a shear modulus of 9.15 ± 0.17 kPa for the upper and 39.05 ± 2.54 kPa for the lower compartment.

Test image

The shear moduli reconstructed from the test data in areas of local homogeneity were 18.8 kPa for the inclusion and 8.4 kPa for the surrounding area [Fig. 2(B)], in perfect agreement with the correct values.

In vivo examinations

Examples of acquired phase images with slice orientations are shown in Figs 4–6 for the examination of the biceps, the flexor digitorum profundus and the calf muscles, respectively. The mean shear modulus values of the seven repeated examinations were 11.3 ± 1.7 and 13.3 ± 4.7 kPa for the two volunteers, respectively (Fig. 7).

Average shear moduli within an ROI were determined to be 17.9 (± 5.5), 8.7 (± 2.8), 12.5 (± 7.3) and 9.9 (± 6.8) kPa for the biceps brachii [Fig. 8(A)], flexor digitorum profundus [Fig. 8(B)], soleus [Fig. 8(C)] and gastrocnemius [Fig. 8(D)], respectively. The results of all examinations are summarized in Table 1. Comparing the average shear moduli of females with males, the results were 18.9 (± 3.7) vs 17.5 (± 6.4) kPa, 8.1 (± 3.3) vs 9.0 (± 2.8) kPa, 9.0 (± 2.6) vs 14.3 (± 8.4) kPa, and 7.4 (± 4.4) vs 11.1 (± 7.7) kPa for the four different muscles.

The statistical analysis yielded statistically significant differences in muscle elasticity (threshold of significance = 5%) in the comparison of the biceps with the flexor digitorum profundus, the soleus, and the gastrocnemius for the group of female volunteers (p-values 0.02, 0.03 and 0.001, respectively), and in the comparison of the biceps with the flexor digitorum profundus for the group of male volunteers (p-value 0.02). Independent of gender, this resulted in a significantly different elasticity of the biceps in comparison to each of the other muscles. The test for the female subgroup also yielded a statistical significance in the comparison of the upper with the lower extremities (p-value 0.04). The comparison between female and male volunteers did not show any statistical significance for any test. The p-values for all tests are summarized in Tables 2 and 3.

No obvious correlations between muscle stiffness and height or weight could be found. The largest correlation coefficient r was 0.43 for weight in the soleus muscle.

DISCUSSION

Agar phantom

The mean values agree roughly with the values determined by the manual wavelength measurement in the acquired phase images. The manual measurement is an inexact method, but can give quick elasticity approximations. One problem with the manual measurement is determining the direction of wave propagation. The

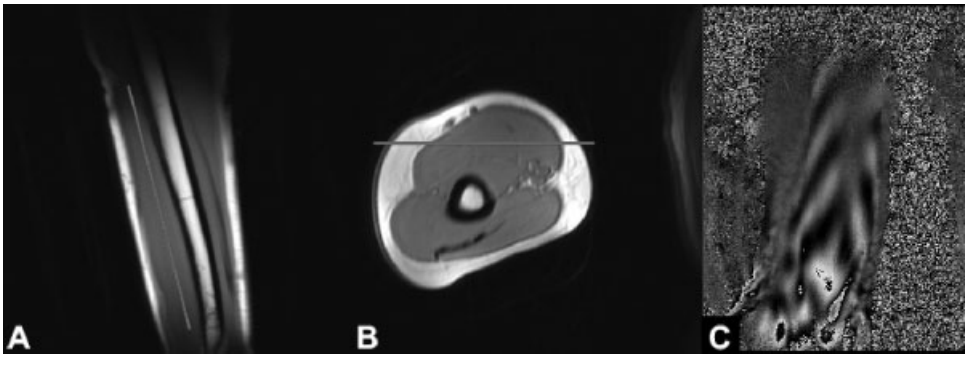

Figure 4. Images of the upper arm acquired with a two-dimensional FLASH sequence in the (A) sagittal and (B) axial planes. (C) The phase image acquired in a coronal slice with orientation corresponding to the red lines in (A) and (B)

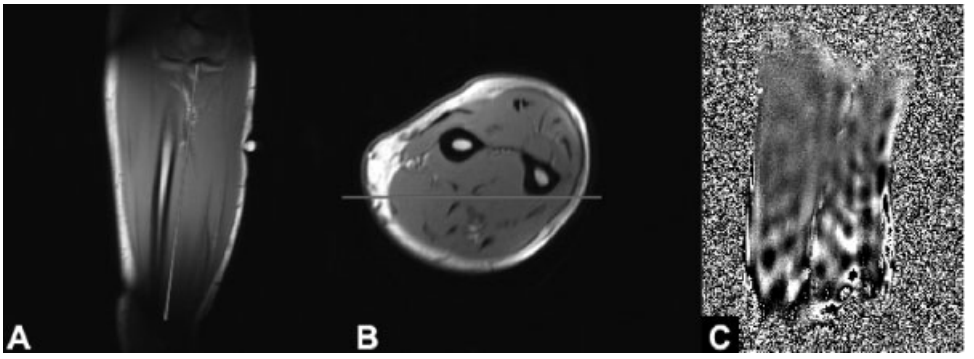

Figure 5. Images of the forearm acquired with a two-dimensional FLASH sequence in the (A) sagittal and (B) axial planes. (C) The phase image acquired in a coronal slice with orientation corresponding to the red lines in (A) and (B)

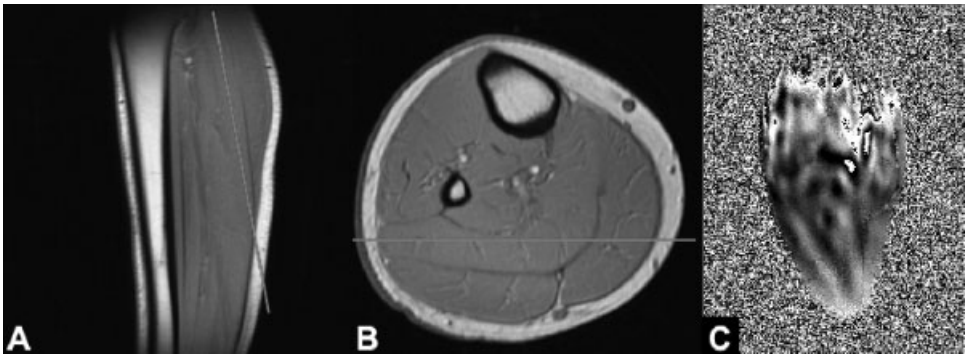

Figure 6. Images of the calf acquired with a two-dimensional FLASH sequence in the (A) sagittal and (B) axial planes. (C) The phase image acquired in a coronal slice with orientation corresponding to the red lines in (A) and (B)

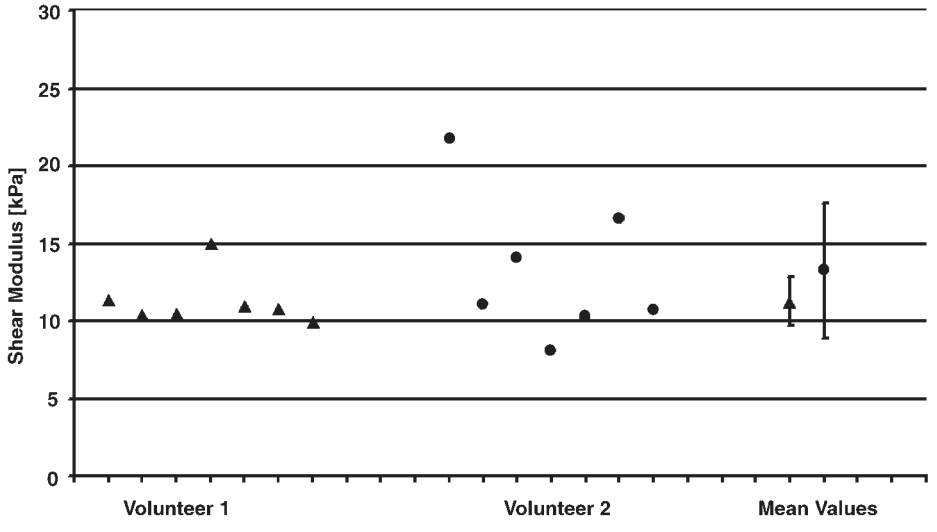

Figure 7. Elasticity values of the seven repeated measurements in the biceps brachii of two volunteers acquired over a span of 8 months. Shear moduli marked with a triangle denote the first volunteer and the ones with circles the second volunteer. The same symbols with error bars represent the mean elasticity values of the two volunteers, respectively. The error bar lengths are the standard deviations over the seven measurements

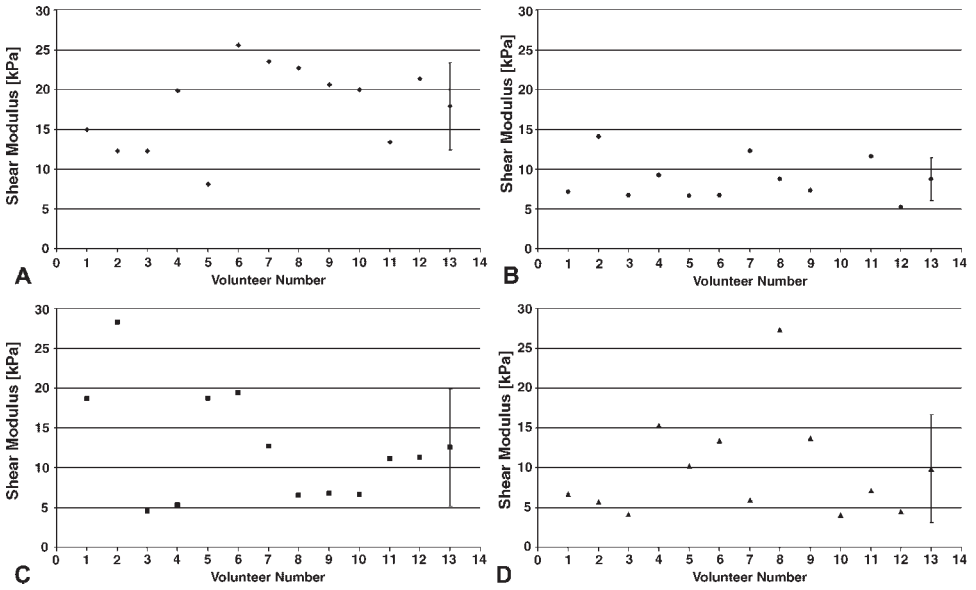

Figure 8. Elasticity values for all volunteers in the (A) biceps brachii, (B) flexor digitorum profundus, (C) soleus and (D) gastrocnemius. Volunteers 1–8 are male and volunteers 9–12 are female. Volunteer 13 gives the mean elasticity and standard deviation over all volunteers

automated method identifies the maximum gradient by using slope measurements in all three dimensions, including through-plane changes.

Hamhaber *et al.*[18] have determined elasticity values for agar gel at different concentrations via mechanical testing. For 1 and 2% gel, they found shear moduli of $\sim$15 and $\sim$56 kPa, respectively. The values found here undershoot these values. They are in acceptable agreement, however, if one takes into account that the type of agar gel used here may have been different from the published data and the exact preparation process also may have influenced the elasticity of the agar gel.

Although both compartments consist of homogenous material, the wave patterns in the phase images are still detectable in the reconstructed data. These artifacts can be filtered out by averaging over a region of interest. This problem arises where constructive interference from reflected waves causes a gain of the amplitude. This amplitude gain leads to a periodical deviation of the spatial phase, which results in elastogram deviations that are further amplified due to the shear modulus proportionality to $1/k^2$. Additional deviations from homogeneity can be detected at the edges of the phantom. There are also artifacts in the reconstruction which arise from wave reflections at the boundaries. Thus, the reconstruction is most reliable under the assumption of homogenous tissue with few sources of reflections, where mean values may be determined over extended regions of the computed elastograms covering several wave cycles. Homogeneity is commonly assumed for muscle tissue. Owing to these weak points in the reconstruction algorithm, the regions for evaluating the *in vivo* phase images were chosen in areas where no wave interference patterns were detectable by visual inspection. This probably led to inaccuracies in muscles like the soleus or the flexor digitorum profundus, where the intersection area of the acquired images with the muscle was fairly small.

Test Image

The test data without any noise or other irregular wave patterns were reconstructed correctly. This simply demonstrates the mathematical correctness of the reconstruction algorithm. The only artifacts arise at boundaries between regions, which represent unnaturally steep changes in elasticity from one pixel to adjacent pixels. As the *in vivo* phase images are evaluated in an inner region of the muscles, where the elasticity is assumed to be homogeneous, these boundary errors are not relevant for the reconstruction of the *in vivo* data.

In vivo examinations

The repeated measurements in the arms of two subjects showed a standard deviation of 1.7 and 4.7 kPa. Interestingly, the measurements in volunteer 1 were very consistent, with the exception of one measurement. The measurements in volunteer 2, although obtained on the same days and with the same setup as volunteer 1, show much greater variability. The source of these variations is unclear. Variations in the setup and positioning of the subject might influence the measurements. It has been demonstrated[8,9] that muscle elasticity is strongly influenced by the load on the muscle. Although all of the exams were nominally performed unloaded, the subjects might have altered the tension in the muscle by working

Table 1. Shear moduli (kPa) for all examinations in each muscle including the standard deviation of the values inside the ROI. Volunteers 1–8 are males and 9–12 are females. The values of the weight and height are given in kg and cm, respectively

Muscle	Volunteer number											
	1	2	3	4	5	6	7	8	9	10	11	12	Mean
Weight	90	83	86	67	78	80	84	72	72	74	58	51	
Height	190	180	188	170	184	168	181	183	176	174	166	160	
Biceps brachii	15.0 ± 4.2	12.3 ± 4.5	12.3 ± 3.2	19.9 ± 5.3	8.1 ± 1.8	25.6 ± 9.4	23.6 ± 6.5	22.8 ± 11.4	20.6 ± 4.5	20.0 ± 4.9	13.5 ± 3.7	21.4 ± 4.6	17.9 ± 5.5
Flexor digitorum profundus	7.2 ± 1.0	14.1 ± 2.2	6.8 ± 0.8	9.2 ± 1.3	6.7 ± 0.5	6.8 ± 1.3	12.3 ± 1.3	8.8 ± 1.1	7.3 ± 1.5	—	11.6 ± 2.5	5.2 ± 0.8	8.7 ± 2.8
Soleus	18.7 ± 2.8	28.3 ± 3.2	4.6 ± 0.3	5.4 ± 0.6	18.8 ± 3.7	19.4 ± 3.9	12.8 ± 1.3	6.5 ± 0.4	6.8 ± 0.8	6.7 ± 0.8	11.2 ± 1.7	11.3 ± 2.2	12.6 ± 7.3
Gastrocnemius	6.7 ± 0.7	5.8 ± 0.4	4.2 ± 0.2	15.3 ± 1.2	10.3 ± 1.0	13.5 ± 1.1	6.0 ± 0.4	27.4 ± 1.1	13.7 ± 0.7	4.2 ± 0.2	7.2 ± 1.2	4.6 ± 0.5	9.9 ± 6.8

Table 2. *p*-values from all Fisher-PLSD tests. Comparison of muscle elasticity between male and female volunteers for each muscle separately, for upper and lower extremity muscles, and for all muscles together

	Biceps	Flexor digitorum profundus	Soleus	Gastrocnemius	Upper extremity	Lower extremity	All muscles
Male ↔ female	0.694	0.660	0.257	0.395	0.732	0.143	0.363

Table 3. *p*-values from all Fisher-PLSD tests. Comparison of all muscles to each other, as well as the upper to the lower extremity muscles, for the female and male subgroups and for both groups together. *p*-Values lower than 0.05 yielded statistical significance and are in italics

	Female	Male	Both
Biceps ↔ flexor digitorum profundus	*0.002*	*0.017*	*0.006*
Biceps ↔ soleus	*0.003*	0.354	*0.031*
Biceps ↔ gastrocnemius	*0.001*	0.069	*0.002*
Flexor digitorum profundus ↔ soleus	0.740	0.122	0.131
Flexor digitorum profundus ↔ gastrocnemius	0.812	0.523	0.640
Gastrocnemius ↔ soleus	0.541	0.351	0.281
Upper ↔ lower extremity	*0.041*	0.848	0.245

against contractions of the opposed muscles. Changes in the wave patterns from interferences due to reflections might also have corrupted the reconstruction, as shown at the edges in the phantom experiment.

However, the elasticity variations might also be explainable by the state of the muscle tissue itself. Little is known about *in vivo* muscle elasticity and its variation over time. The momentary elasticity might be determined by the history of muscle use preceding the examination for a period of hours to days, or on the hydration or biochemical state of the subject. The influence of sport and exercise will have to be further investigated. These natural fluctuations may make it difficult to increase the precision of MRE measurements over time.

Previous studies yielded shear moduli of the biceps from 14 to 39 kPa.[8,14] Examinations performed by Basford *et al.*[10] determined the mean shear modulus of the soleus to be 17 kPa and that of the gastrocnemius lateralis to be 16 kPa. A study with sonoelasticity by Levinson *et al.*[1] yielded a Young's modulus of 79 kPa in the quadriceps, corresponding to a shear modulus of around 27 kPa. It is difficult to compare these results directly, but the elasticity values all fall into similar ranges. As far as documented in the aforementioned studies, the muscles weren't under load. Given the large variability among even healthy tissue, larger studies would be needed to more precisely determine the range of muscle elasticity.

The mean elasticity values of the four individual muscles are strongly scattered. The standard deviations range from 5.5 kPa in the biceps up to 7.3 kPa in the soleus. No trend is notable in the shear modulus values between muscles, so that a differentiation by muscle volume, muscle fiber type, muscle function or other specific muscle characteristics is unclear.

The results of the statistical analysis revealed a general difference between the biceps and the flexor digitorum profundus in both males and females. A possible explanation could be that the biceps, with the higher average

shear modulus, is required to generate higher forces compared with the muscles moving the fingers. The statistical tests also showed significant difference between the biceps and both of the lower extremity muscles of the female volunteers, who had a comparable biceps stiffness to men but a lower shear modulus in the calf muscles. No correlation between leg muscle stiffness and height and weight was found, so perhaps the difference in lower extremity muscle stiffness is due to hormonal or other differences. However, since a correlation to weight or height is expected, a higher number of volunteers is needed to clarify the tendency in the data related to weight and height.

Although the reconstruction algorithm introduced here exhibits weaknesses, the deviations are systematic and can be assumed to lead to equivalent deviations in the reconstruction of phase images acquired with the same orientation and parameters. The manual image analysis is extremely difficult within complex wave patterns, where the direction of propagation is not obvious, e.g. in the calf muscles. Small angles between the direction of the wave vector and the direction of the measurement by hand lead to significant variations of the wavelength measurement.

The reconstruction assumptions of an extended, Hookean, isotropic medium are not valid for skeletal muscle tissue, but these assumptions are generally assumed to yield an acceptable estimation of the elasticity, as represented by the shear modulus. To better adapt the reconstruction to the characteristics of skeletal muscle, e.g. anisotropy, the reconstruction of the elasticity tensor is required, which has already been performed on female breast data to investigate elastic anisotropy.[6] This would include the acquisition of a dataset with the motion-sensitizing gradients in all three spatial directions. The eigenvectors of the elasticity tensor would most likely reveal information about the orientation of the muscle fiber axes, since it is expected that the elasticity is different along the fiber axis than in the orthogonal directions. An examination time of at least 45 min would be required using the current pulse sequence, but the enhancements in data evaluation, including anisotropy and muscle fiber tracking, would open new aspects for studying skeletal muscle.

CONCLUSION

This study confirms that MRE represents a unique possibility to measure muscle tissue elasticity *in situ*. As so little is known about tissue elasticity and its normal variation in the population and its dependence on factors such as age, activity and diet, there is currently a need to collect data similar to those presented here to establish more concretely the influences on tissue elasticity. The series of repeated same-subject examinations needs to be continued to get better insight into how the experimental setup influences measurement precision and to determine which external factors may affect elasticity over time.

Given that the elasticity values in healthy subjects vary substantially, it remains to be investigated what deductions can be reached in patients with muscle pathology or injury. A small initial study has already demonstrated significant differences in patients with paraplegia or history of poliomyelitis.[10] The measurements in the study of Basford *et al.*[10] were performed with a passive ankle torque applied to the calf muscle. Reproducibility and elasticity variations should be investigated with such a setup in both upper and lower extremity muscles, including a larger number of healthy volunteers. A further improvement might be to adapt the load to each individual. This could be realized by asking the subject to actively maintain a constant force at a given fraction of his or her maximum voluntarily generated force. Adaptation of the force has the advantage that it is consistently applicable, even in diseased patients.

Additionally, more needs to be understood about variations in more specialized segments of the healthy population, including subjects with special muscle characteristics due to profession or competitive sports, e.g. sprinters and long distance runners. This would determine how strongly elasticity is directly influenced by muscle use or muscle fiber type. Biometric quantities other than weight and height, such as muscle volume or cross-sectional area, should also be included in the analysis.

Although the baseline information gathered here is a good start, the proposed continuative experiments could help clarify influences on the mechanical properties of skeletal muscle and will be essential for determining the potential of skeletal muscle MRE with regard to clinical practice.

Acknowledgments

This work was supported by a grant from the Ministry for Science and Research of the state of North Rhine-Westphalia, Germany. We would like to thank the employees of the Department of Physiotherapy of the University Hospital Essen for their support and participation in this study.

REFERENCES

1. Levinson SF, Shinagawa M, Sato T. Sonoelastic determination of human skeletal muscle elasticity. *J. Biomech.* 1995; **28**(10): 1145–1154.
2. Muthupillai R, Lomas DJ, Rossman PJ, Greenleaf JF, Manduca A, Ehman RL. Magnetic resonance elastography by direct visualization of propagating acoustic strain waves. *Science* 1995; **269**(5232): 1854–1857.
3. Plewes DB, Betty I, Urchuk SN, Soutar I. Visualizing tissue compliance with MR imaging. *J. Magn. Reson. Imag.* 1995; **5**(6): 733–738.

4. Muthupillai R, Rossman PJ, Lomas DJ, Greenleaf JF, Riederer SJ, Ehman RL. Magnetic resonance imaging of transverse acoustic strain waves. *Magn. Reson. Med.* 1996; **36**(2): 266–274.
5. Kruse SA, Smith JA, Lawrence AJ, Dresner MA, Manduca A, Greenleaf JF, Ehman RL. Tissue characterization using magnetic resonance elastography: preliminary results. *Phys. Med. Biol.* 2000; **45**(6): 1579–1590.
6. Sinkus R, Lorenzen J, Schrader D, Lorenzen M, Dargatz M, Holz D. High-resolution tensor MR elastography for breast tumour detection. *Phys. Med. Biol.* 2000; **45**(6): 1649–1664.
7. Van Houten EE, Doyley MM, Kennedy FE, Weaver JB, Paulsen KD. Initial *in vivo* experience with steady-state subzone-based MR elastography of the human breast. *J. Magn. Reson. Imag.* 2003; **17**(1): 72–85.
8. Dresner MA, Rose GH, Rossman PJ, Muthupillai R, Manduca A, Ehman RL. Magnetic resonance elastography of skeletal muscle. *J. Magn. Reson. Imag.* 2001; **13**(2): 269–276.
9. Uffmann K, Mateiescu S, Quick HH, Ladd ME. *In vivo* determination of biceps elasticity with MR elastography. In *Proceedings of the 10th Annual Meeting of ISMRM*, Honolulu, 2002; 37.
10. Basford JR, Jenkyn TR, An KN, Ehman RL, Heers G, Kaufman KR. Evaluation of healthy and diseased muscle with magnetic resonance elastography. *Arch. Phys. Med. Rehabil.* 2002; **83**(11): 1530–1536.
11. Leroy-Willig A, Carlier P, Morvan D, Duboc D, Fardeau M. Functional imaging of human muscle. *Rev. Neurol. (Paris)* 1998; **154**(5): 379–388.
12. Saab G, Thompson RT, Marsh GD. Multicomponent T_2 relaxation of *in vivo* skeletal muscle. *Magn. Reson. Med.* 1999; **42**(1): 150–157.
13. Bryan WW, Reisch JS, McDonald G, Herbelin LL, Barohn RJ, Fleckenstein JL. Magnetic resonance imaging of muscle in amyotrophic lateral sclerosis. *Neurology* 1998; **51**(1): 110–113.
14. Sack I, Bernarding J, Braun J. Analysis of wave patterns in MR elastography of skeletal muscle using coupled harmonic oscillator simulations. *Magn. Reson. Imag.* 2002; **20**(1): 95–104.
15. Uffmann K, Abicht C, Grote W, Quick HH, Ladd ME. Design of an MR-compatible piezoelectric actuator for MR elastography. *Con. Magn. Reson. (Magn. Reson. Eng.)* 2002; **15**(4): 239–254.
16. Elmore WC, Heald MA. *Physics of Waves*. Dover: New York, 1969.
17. Burlew MM, Madsen EL, Zagzebski JA, Banjavic RA, Sum SW. A new ultrasound tissue-equivalent material. *Radiology* 1980; **134**(2): 517–520.
18. Hamhaber U, Grieshaber FA, Nagel JH, Klose U. Comparison of quantitative shear wave MR-elastography with mechanical compression tests. *Magn. Reson. Med.* 2003; **49**(1): 71–77.

